PHILOSOPHICAL TRANSACTIONS OF THE ROYAL SOCIETY A

Phil. Trans. R. Soc. A (2010) **368**, 4419–4437
doi:10.1098/rsta.2010.0133

Characterization of magnetic nanoparticles using programmed quadrupole magnetic field-flow fractionation

By P. Stephen Williams*, Francesca Carpino† and Maciej Zborowski

Department of Biomedical Engineering, Lerner Research Institute, Cleveland Clinic, 9500 Euclid Avenue, Cleveland, OH 44195, USA

Quadrupole magnetic field-flow fractionation is a relatively new technique for the separation and characterization of magnetic nanoparticles. Magnetic nanoparticles are often of composite nature having a magnetic component, which may be a very finely divided material, and a polymeric or other material coating that incorporates this magnetic material and stabilizes the particles in suspension. There may be other components such as antibodies on the surface for specific binding to biological cells, or chemotherapeutic drugs for magnetic drug delivery. Magnetic field-flow fractionation (MgFFF) has the potential for determining the distribution of the magnetic material among the particles in a given sample. MgFFF differs from most other forms of field-flow fractionation in that the magnetic field that brings about particle separation induces magnetic dipole moments in the nanoparticles, and these potentially can interact with one another and perturb the separation. This aspect is examined in the present work. Samples of magnetic nanoparticles were analysed under different experimental conditions to determine the sensitivity of the method to variation of conditions. The results are shown to be consistent and insensitive to conditions, although magnetite content appeared to be somewhat higher than expected.

Keywords: magnetic nanoparticles; field-flow fractionation; characterization; quadrupole magnet; magnetic field-flow fractionation; magnetic dipole interaction

1. Introduction

The technique of field-flow fractionation (FFF) was invented in 1966 by J. Calvin Giddings (Giddings 1966). It is a separation and characterization technique for macromolecules, nanoparticles and larger particles of up to around 100 μm in diameter. As it was conceived, separation takes place within a flow of suspending fluid passing through a thin, parallel-walled channel across the thickness of which a field or field gradient is applied. The channel must have uniform thickness across its breadth, and the field or field gradient must also be uniform across the channel breadth. It is an elution technique like chromatography in that different sample

*Author for correspondence (willias3@ccf.org).
†Present address: Department of Chemical and Biomolecular Engineering, 325 Stinson-Remick Hall, University of Notre Dame, Notre Dame, IN 46556, USA.

One contribution of 14 to a Theme Issue 'Nanoparticles'.

components are carried at different rates to a detector at the channel outlet. The mechanism of separation has been described in the literature (e.g. Giddings 1984, 1993, 2000).

Magnetic field-flow fractionation (MgFFF) is a relatively new form of FFF. Early attempts to develop MgFFF were not generally very successful for various reasons principally associated with non-ideal channel geometry and field arrangements. The literature concerning these early attempts has been described by us previously (Carpino *et al.* 2005*a*,*b*; Williams *et al.* 2009*a*). It was noted above that FFF optimally requires the field and/or field gradient to be uniform across the breadth of the channel, and that the channel also be of uniform thickness across its breadth. An exception to this arrangement of a thin channel of uniform thickness with a transverse field is the axisymmetrical symmetry of hollow fibre FFF, where a fraction of the fluid flows radially outward through the permeable fibre wall (Jönsson & Carlshaf 1989; Wijnhoven *et al.* 1995; Reschiglian *et al.* 2005). On the other hand, a tubular channel with transverse field is not a suitable design for FFF, as explained by Giddings (2000). Nevertheless, attempts at development of MgFFF based on this arrangement have been described in the literature (Vickrey & Garcia-Ramirez 1980; Mori 1986; Latham *et al.* 2005).

We have taken a very different approach to development of MgFFF. For MgFFF, it is advantageous to employ a quadrupole, or higher order, magnetic field. Such magnet systems exhibit axisymmetrical symmetry for the magnitude of the magnetic field within the aperture. The direction of the field changes with characteristic periodicity, but its magnitude is constant at any radial distance from the axis. In the case of the quadrupole magnet, the field magnitude increases linearly from the axis so that the gradient in field magnitude is constant within the aperture and is directed away from the axis (Zborowski 1997; Zborowski *et al.* 1999). Practicality precludes the use of a tubular capillary channel with correspondingly small quadrupole aperture. For a larger aperture quadrupole, the channel is better confined to a thin annular space close to the pole pieces where the field magnitude is highest. The channel may occupy the full annulus, but such a design suffers from the associated difficulty of arranging uniform channel flow. Very small variations in annular thickness, or non-uniform introduction or collection of fluid around the annulus would strongly disturb the flow symmetry and, consequently, the separation (Williams *et al.* 2002; Carpino *et al.* 2005*a*,*b*). A solution is to confine the channel to a fraction of the annulus, or alternatively, to use a helical channel within the annular space. We have chosen the latter approach, as it has the benefit of compensating for any small variations in field gradient around the aperture. In either case, a single inlet and a single outlet is sufficient to distribute fluid to and collect fluid from the channel.

It will be shown in the theory section that the force on a particle in a magnetic field gradient is proportional to the volume of the material in the particle that interacts with the field. This is also true of particles in a centrifugal field. The result of this is a very high size-selectivity for both sedimentation field-flow fractionation (SdFFF) and MgFFF separations—elution time increases with the cube of particle diameter. More correctly, elution time increases with the cube of the diameter of a sphere of volume equal to that of the material within a particle that interacts with the field. This may be referred to as the equivalent spherical core diameter where it is only the core material that interacts with the field, and this material may be finely divided and distributed within the total

volume of the particle. During the early development of SdFFF, it was quickly realized that because of the high selectivity, a constant field is not suitable for the analysis of polydisperse samples, and it is necessary to use a programmed field decay during sample elution (Yang *et al.* 1974; Kirkland *et al.* 1981; Giddings *et al.* 1987; Williams & Giddings 1987). This is also true of MgFFF, and it is necessary to program the decay of field and field gradient using a quadrupole electromagnet and computer control of the current supply.

It will also be explained in the theory section that in MgFFF, the induced magnetic moments of the particles not only interact with the field gradient, but also can potentially interact with one another. Ideal FFF retention theory requires that particle–particle interactions are insignificant. Conditions giving rise to significant interactions will result in perturbations to particle elution and errors in quantitative information extracted on the assumption of ideal behaviour. A further complication is the use of programmed field decay. Conditions may give rise to significant particle dipole–dipole interactions at a high initial field, but these interactions may become less significant as the field decays. The influence of fluid shear rate on interactions between suspended magnetic dipoles will also be discussed in §2. The shear rate at the accumulation wall is of course directly related to the channel flow rate. It is possible that the perturbations to particle elution times may be functions of flow rate as well as programmed field conditions.

The work described in this study involves the analysis of magnetic nanoparticle materials using a number of different field-decay and flow-rate conditions. The objective is to determine the consistency, or lack thereof, of the calculated distributions in magnetite content, expressed as equivalent spherical magnetite core diameters.

2. Theory

The ideal model of elution in the normal mode of FFF is based on a number of assumptions that are good for most of the FFF techniques, at least when conditions are arranged to minimize perturbations. For example, a thin channel must have a high enough cross-sectional aspect ratio that the fluid velocity profile is uniform across the majority of its breadth. The particles are assumed to be of negligible size compared with the zone thickness, and therefore the channel. It is however simple to include first-order corrections to account for finite particle size (Giddings 1978; Giddings 1979; Williams & Giddings 1994). It is also assumed that there are negligible particle–wall and particle–particle interactions (Hansen & Giddings 1989; Hansen *et al.* 1989; Williams *et al.* 1997). These may be good assumptions when sample concentration is sufficiently low, and when carrier fluid composition is optimized in terms of pH, ionic strength, and surfactant composition and concentration. MgFFF, however, differs from most forms of FFF in that under the influence of the magnetic field, a magnetic dipole moment is induced in the particles. The magnetic moments tend to be aligned with the magnetic field, and depending on their relative positions in space and with respect to the field direction, a pair of particles may attract or repel one another. Under certain conditions, this effect may influence the elution of the particles. We shall return to this aspect, but first, the equations describing elution where there is negligible dipole–dipole interaction will be presented.

(*a*) *Ideal elution model for magnetic field-flow fractionation*

The force $\mathbf{F}_\mathrm{m}$ on a magnetized particle in a magnetic field gradient is given by the equation

$$\mathbf{F}_\mathrm{m} = V_\mathrm{m} M \boldsymbol{\nabla} B, \tag{2.1}$$

where V_m is the volume of magnetized material incorporated in the particle, M is the magnetization of this material in the magnetic field and $\boldsymbol{\nabla} B$ is the gradient in magnetic field B. The magnetized component is typically magnetite, maghemite or some other material that strongly interacts with a magnetic field. It is assumed that other components such as polymeric coatings or surfactants for suspension stabilization, as well as antibodies or incorporated drugs, and the suspending fluid have negligible interaction with the field. Note that $\mathbf{F}_\mathrm{m}$ is in bold face to indicate that it is a vector quantity. For the thin helical channel mounted axisymmetrically in the quadrupole field, we can assume that the force is directed away from the axis, across the channel thickness toward the outer accumulation wall. If the radius of the outer channel wall is represented by r_o and the magnitude of the field at the outer channel wall by B_o, then $\boldsymbol{\nabla} B = B_\mathrm{o}/r_\mathrm{o}$, and we have

$$F_\mathrm{m} = \frac{V_\mathrm{m} M B_\mathrm{o}}{r_\mathrm{o}}. \tag{2.2}$$

Equation (2.2) shows that F_m is a function of the magnetization M of the magnetic component, which is in turn a function of local magnetic field B. However, the particles are confined to a thin annular space, across which the magnitude of the field will vary by, typically, a few percent. Furthermore, the particles are confined to a thin zone within this annular space next to the outer (accumulation) wall. We can therefore assume the force experienced by the particles across the zone thickness corresponds to that at the accumulation wall, without introducing significant error. The steady-state concentration profile across the channel thickness is found to be given by (Williams *et al.* 2009*b*)

$$c = c_\mathrm{o} \exp\left(-\frac{\xi}{\lambda}\right), \tag{2.3}$$

in which c_o is the concentration next to the accumulation wall, ξ is the fractional distance across the channel thickness from the accumulation wall and

$$\lambda = \frac{kT}{W_\mathrm{o}} = \frac{kT}{F_\mathrm{m} w} = \frac{kT r_\mathrm{o}}{V_\mathrm{m} M B_\mathrm{o} w}. \tag{2.4}$$

The parameter λ is the so-called retention parameter in FFF. It is the ratio of thermal energy kT (k is the Boltzmann constant and T the absolute temperature) to the work W_o required to drive a particle across the channel thickness w against the magnetic force F_m. Therefore, in the ideal case, the concentration profile is expected to decay exponentially away from the accumulation wall.

For an elution technique, elution times are recorded rather than elution velocities, and the elution time, or alternatively, the retention time is predicted in terms of the retention ratio R. This is the ratio of the mean time t^0 for the fluid to pass through the channel (known as the void time) to that for the retained material t_r. This is equivalent to the ratio of the velocity of the retained material v_p to the mean velocity of the fluid $\langle v \rangle$. The assumption of a parabolic fluid

velocity profile across the thin channel leads to the familiar equation for the FFF retention ratio,

$$R = \frac{t^0}{t_r} = \frac{v_p}{\langle v \rangle} = 6\lambda(\coth(1/2\lambda) - 2\lambda) \approx 6\lambda(1 - 2\lambda), \tag{2.5}$$

where the final approximate form is accurate to 0.36 per cent for λ up to 0.15 or R up to 0.63. The consideration of a first-order correction for finite particle size (Giddings 1978) yields the equation

$$\begin{aligned} R &= 6\alpha(1-\alpha) + 6\lambda\left\{(1-2\alpha)\coth\left(\frac{1-2\alpha}{2\lambda}\right) - 2\lambda\right\} \\ &\approx 6\alpha(1-\alpha) + 6\lambda(1-2\alpha-2\lambda), \end{aligned} \tag{2.6}$$

in which α is the ratio of particle radius to channel thickness, or $d_p/2w$, and the final approximate form is again accurate for small λ.

(*b*) *Field and field-gradient programming for magnetic field-flow fractionation*

It was already mentioned that field-gradient-decay programming is generally necessary for magnetic nanoparticle analysis by MgFFF. The magnetic field and field gradient are generally related, and in the quadrupole field, the relationship is very simple: $\nabla B = B_o/r_o$. A programmed decay of the field at the channel accumulation wall results in a proportional decay of the field gradient. For reasons that we do not have to go into here, the field-decay program for analysis of a polydisperse sample should ideally approach zero field asymptotically (Williams *et al.* 1987). Such programs include the exponential and power programs (Kirkland *et al.* 1981; Yau & Kirkland 1981; Giddings *et al.* 1987; Williams & Giddings 1987, 1991, 1994). We choose the power program for its flexibility and potential for uniform relative resolution over a wide range. This takes the form

$$B_o(t) = B_o(0)\left(\frac{t_1 - t_a}{t - t_a}\right)^p, \tag{2.7}$$

in which $B_o(t)$ is the field at the accumulation wall at time t, $B_o(0)$ is the initial field that is held constant for a pre-decay time t_1, t_a is a second time constant that is commonly set to $-pt_1$ and p is some positive number.

Equation (2.2) shows that the force on a particle is a function of both the field gradient and the magnetization of the material that responds to the field. This is unlike other forms of FFF where optimization of programming conditions, including the value of the power p, is more straightforward. For example, in SdFFF where λ is inversely dependent on the cube of particle diameter, the optimum p giving constant diameter-based fractionating power (a measure of relative resolving power) may be shown to be eight (Williams & Giddings 1987). This would be true of MgFFF if magnetization was not also a function of applied field (see equations (2.2) and (2.4)). However, we are not concerned with the optimization of programmed conditions in this work. This will be considered elsewhere.

(c) Data reduction for magnetic field-flow fractionation

Data reduction for FFF is concerned with the transformation of an elution profile of detector response versus elution time into a distribution in terms of a selective parameter such as particle size. A generalized approach to data reduction for FFF has been described in the literature (Williams *et al.* 2001). The approach for MgFFF is a little more complicated than for other forms of FFF because of the dependence of magnetization on the applied field. Nevertheless, the general approach may be followed, with calculations taking into account the continuous changes in λ and therefore R for the range of V_m, or alternatively, equivalent spherical core diameters d_m, where $d_\mathrm{m} = (6\,V_\mathrm{m}/\pi)^{1/3}$.

From equation (2.5), we have the zone velocity for particles of some given d_m at some instant during elution given by

$$v_\mathrm{p} = R\langle v\rangle, \tag{2.8}$$

where R is a function of λ, which is in turn a function of B_o and M, which is also a function of B_o. The zone will elute from the channel at some elution time t_r, and the distance travelled in this time must correspond to the length of the channel L. It follows that

$$L = \int_0^{t_\mathrm{r}} v_\mathrm{p}\,\mathrm{d}t = \int_0^{t_\mathrm{r}} R\langle v\rangle\,\mathrm{d}t. \tag{2.9}$$

The experiments reported in this work involve the programming of only the field, and the channel flow rate was held constant. The void time t^0 is simply the channel length L divided by the mean fluid velocity $\langle v\rangle$, and equation (2.9) reduces to

$$\int_0^{t_\mathrm{r}} R\,\mathrm{d}t - t^0 = 0. \tag{2.10}$$

If we include the specific functional dependencies on the experimental parameters, we have

$$\int_0^{t_\mathrm{r}} R(B_\mathrm{o}(t), M(B_\mathrm{o}(t)), d_\mathrm{m})\,\mathrm{d}t - t^0 = 0, \tag{2.11}$$

where it is assumed that T, r_o and w are known and are fixed. If a steric correction for R is to be considered, then an assumption concerning its dependence on d_m must be made.

During a sample analysis, the values of detector response $h(i)$ and applied field $B_\mathrm{o}(i)$ are recorded to a data file at discrete intervals of time $t(i)$. The approach then requires equation (2.11) be solved numerically for t_r for a set of discrete values of d_m, taking into account the recorded dependence of B_o on t, and a real or assumed dependence of M on B_o. An adaptive method is followed to ensure an even distribution of these discrete d_m across the range of eluted material (see Williams *et al.* 2001). It is then a matter of interpolation to associate a value of $d_\mathrm{m}(i)$ with every discrete elution time $t_\mathrm{r}(i)$ in the data file for which a solution is found. (Note that the discrete times $t(i)$ correspond to discrete elution times $t_\mathrm{r}(i)$ when associated with a detector response.) Finally, the transformation to a particle mass distribution in d_m must be made.

Suppose $m(d_{\mathrm{m}}(i))$ represents the mass of particles having equivalent spherical core diameters between $d_{\mathrm{m}}(i)$ and $d_{\mathrm{m}}(i) + \delta d_{\mathrm{m}}$. It follows that

$$m(d_{\mathrm{m}}(i)) = c(i)\,\dot{V}\frac{\delta t_{\mathrm{r}}(i)}{\delta d_{\mathrm{m}}}, \tag{2.12}$$

where $c(i)$ is the mass concentration of particles eluting at time $t_{\mathrm{r}}(i)$, and $\delta t_{\mathrm{r}}(i)$ is the difference in elution time for particles of $d_{\mathrm{m}}(i)$ and $d_{\mathrm{m}}(i) + \delta d_{\mathrm{m}}$, and $\dot{V}$ is the volumetric channel flow rate. Note that the transformation corresponding to equation (2.12) does not account for the band broadening that occurs during sample elution. However, the high selectivity of the FFF separation, even under the programmed field-decay conditions, means that the breadth of a peak for a polydisperse sample is dominated by the polydispersity (Martin *et al.* 1979). Furthermore, it has been shown that correction of peak shape by deconvoluting the non-equilibrium band broadening (the dominant contribution to system dispersion) has relatively little effect on the calculated distributions of polydisperse samples (Schimpf *et al.* 1989). Note also that for the work reported here, a UV detector was used and the relationship between detector response $h(i)$ and mass concentration of particles $c(i)$ is not known. However, the objective of this work is the comparison of equivalent spherical core-diameter distributions obtained under differing programmed field and flow conditions, and the comparison is perfectly valid without the conversion of $h(i)$ to $c(i)$. Equivalent distributions will have equivalent biases in core sizes.

(*d*) *Magnetic dipole interactions in magnetic field-flow fractionation*

As we have explained, MgFFF differs from most other forms of FFF in that a magnetic moment is induced in the particles by the applied magnetic field, and the magnetic moment interacts with the field gradient to induce particle migration. The particle magnetic dipoles have the potential to interact with one another, and this may perturb particle elution.

Ferrofluids are composed of colloidal, single-domain ferromagnetic particles suspended in a fluid. It is energetically favourable for magnetic materials to be divided into small domains having uniform magnetizations aligned in different directions. Particles tend to be single domain when smaller than some critical size where energy considerations no longer favour their division into more than one domain. They therefore contain no domain walls, and within a particle, atomic magnetic moments are all aligned with one another. The particles have zero coercivity and the direction of magnetization can randomly flip, even under the influence of thermal energy. The particles do have permanent magnetic moments that may interact with one another, and they are commonly stabilized in suspension by thin, molecular coatings. It was predicted that such particles would interact to form chains even at zero applied magnetic field, and that under an applied field, they would form longer chains which align with the field (de Gennes & Pincus 1970; Jordan 1973). Such chains were observed by Hayes (1975) and by Chantrell *et al.* (1982).

The magnetic nanoparticles analysed by MgFFF in this study contain multiple, single-domain magnetite crystals. When not subjected to a magnetic field, the crystal dipole moments will be randomly oriented and be constantly changing direction under the influence of thermal energy. The particles do not then carry an

overall magnetic dipole moment. When a magnetic field is applied, the individual dipoles tend to align with the field and the composite nanoparticles acquire a magnetic dipole moment. They become magnetically saturated when all of the individual dipoles become aligned with the field, and this tends to occur at relatively low fields of around 0.1–0.2 T.

The dipole–dipole interaction energy for a pair of identical spherical magnetized particles, aligned with the applied field, is given by (Rosensweig 1997)

$$E_{\mathrm{dd}} = \frac{\pi}{9}\frac{\mu_0 M_{\mathrm{p}}^2 d^3}{(l+2)^3}, \tag{2.13}$$

where μ_0 is the magnetic permeability of free space ($\mu_0 = 4\pi \times 10^{-7}\,\mathrm{H\,m^{-1}}$), M_{p} is the particle magnetization, d is the particle diameter and $l = 2s\,d^{-1}$, with s being the surface to surface separation distance. It follows that for two identical magnetized particles, having magnetic and non-magnetic components, in contact and aligned with the applied field, the dipole–dipole interaction energy is given by

$$E_{\mathrm{dd}} = \frac{\pi}{72}\frac{\mu_0 M^2 d_{\mathrm{m}}^6}{d_{\mathrm{p}}^3}, \tag{2.14}$$

in which M is the magnetization of the magnetic component of equivalent spherical diameter d_{m}, and d_{p} is the overall diameter of the particles. A so-called coupling constant has been defined as the ratio of this E_{dd} to thermal energy kT (de Gennes & Pincus 1970), and from the point of view of FFF, unfortunately given the symbol λ. We shall define the coupling constant λ_{cc} as

$$\lambda_{\mathrm{cc}} = \frac{E_{\mathrm{dd}}}{kT} = \frac{\pi}{72}\frac{\mu_0 M^2 d_{\mathrm{m}}^6}{kT d_{\mathrm{p}}^3}. \tag{2.15}$$

It may be assumed that particle chaining may be significant when λ_{cc} exceeds unity, and that chains are disrupted by thermal energy when λ_{cc} is much less than unity.

There is another aspect to dipole–dipole interaction that must be considered in the case of MgFFF. The particles are driven close to the accumulation wall and are carried along the channel by a shear flow of fluid. For a spherical particle in an unbounded shear flow, the rotation rate (angular velocity) is equal to half the shear rate (Jeffery 1922). When the particle is close to a bounding wall, the rotation rate is reduced (Goldman *et al.* 1967). The magnetic field has only a small component in the direction across the channel breadth and any chains of magnetized particles will tend to align with the field in a plane perpendicular to the direction across the channel breadth. The shear flow will therefore exert a torque on a chain of magnetized particles and the magnetic field will exert an opposing torque when the chain is out of alignment with the local field. The related situation of magnetized particle chains subjected to rotating magnetic fields has been studied by Melle and co-workers (Calderón & Melle 2002; Melle *et al.* 2000, 2001, 2002*a*,*b*, 2003). These studies involved magnetorheological fluids composed of a suspension of approximately 1 μm diameter latex particles that incorporated randomly oriented 1–20 nm magnetite crystals. They had zero magnetic moment in the absence of a magnetic field. Under the applied fields used in experiments, the values of λ_{cc} (see equation (2.15)) typically fell in the

range of 200–700. At low rotation frequencies, the chains rotated at the same frequency with a small lag behind the magnetic field. With increasing frequency, the average length of the chains decreased and the lag behind the field increased. At still higher frequency, the hydrodynamic friction forces overcame the dipolar magnetic forces, and this caused the chains to break up. They were also able to relate the phase lag of a rotating chain and the chain length to the Mason number, which is a dimensionless number that compares the viscous and the magnetic forces. The Mason number was initially introduced to describe chain formation in electrorheological fluids under shear flow (Gast & Zukoski 1989; Martin & Anderson 1996; Volkova *et al.* 1999). It is defined by Melle *et al.* as

$$\mathrm{Ma} = \frac{12^2 \eta \omega}{\mu_0 M_\mathrm{p}^2}, \tag{2.16}$$

where ω is the frequency of the rotating field. It follows that for particles having magnetic and non-magnetic components

$$\mathrm{Ma} = \frac{12^2 \eta \omega}{\mu_0 M^2} \left(\frac{d_\mathrm{p}}{d_\mathrm{m}} \right)^6, \tag{2.17}$$

in which M is the magnetization of the magnetic material having an equivalent spherical diameter of d_m, and d_p is the overall particle diameter. They showed through simulations that the average chain length decreases approximately with the square root of Ma and falls to around 2 when Ma $\approx$1. These simulations were in agreement with scattering dichroism experiments (Melle *et al.* 2002*a*) and with direct microscopic observations (Melle *et al.* 2003). As mentioned above, for a spherical particle entrained in a shear flow, the rotation rate ω is equal to half the shear rate $\dot{\gamma}$ (Jeffery 1922). For the case of magnetized particles entrained in a shear flow, we may therefore transform equation (2.17) to

$$\mathrm{Ma} = \frac{72 \eta \dot{\gamma}}{\mu_0 M^2} \left(\frac{d_\mathrm{p}}{d_\mathrm{m}} \right)^6. \tag{2.18}$$

3. Experimental

The quadrupole magnetic field-flow fractionation (QMgFFF) system has been described previously (Carpino *et al.* 2005*a*,*b*, 2007; Williams *et al.* 2009*a*). The quadrupole electromagnet was designed and assembled in our laboratory. It consisted of four American Wire Gauge 18 coated copper wire coils, each of nominally 1900 m length, wound around 1018 low-carbon, cold-rolled steel plates, 15.24 cm tall and 2.54 cm thick. The coils were wound by Coil Winding Specialist (CWS, Santa Ana, CA, USA). One end of each plate was machined at the Cleveland Clinic Prototype Laboratory to the required hyperbolic pole-piece profile. The four poles were arranged with opposed N to N and S to S to generate an axisymmetric field gradient in an aperture of 16 mm diameter. The electrical resistances of the copper wire coils were measured and found to be between 35.6 and 35.8 Ω. The coil wire lengths were fine tuned to equalize field at the pole tips, rather than to equalize resistance. The field-return paths were facilitated with a square yoke of 1018 low-carbon, cold-rolled steel. This was also

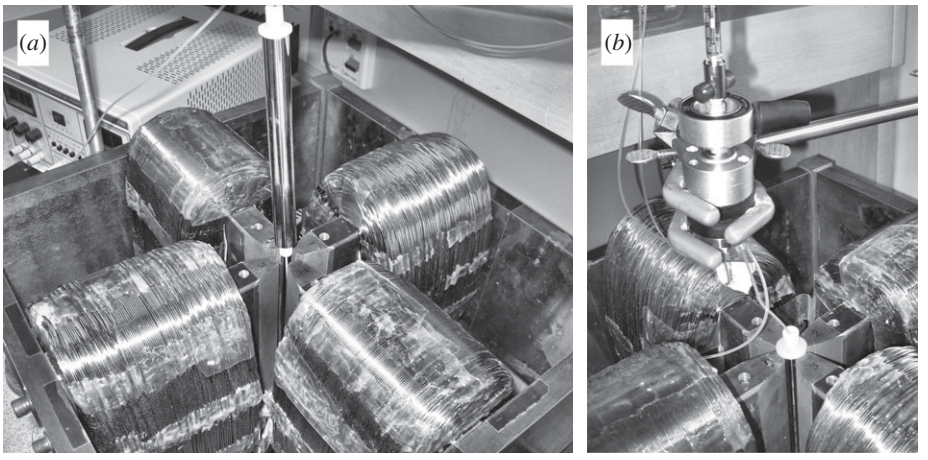

Figure 1. (*a*) The quadrupole electromagnet with the FFF channel held above the aperture and (*b*) the channel inserted into the aperture for sample analysis with the injection valve above.

made of 15.24 cm tall plates, but of 1.91 cm thickness. A schematic of the cross section of the electromagnet plates and coils has been shown in the literature (Carpino *et al.* 2005*b*). A photograph of the quadrupole electromagnet is shown in figure 1*a*. The stainless-steel tube housing the helical FFF channel is shown above the quadrupole aperture. It is lowered into the aperture during experiments for particle analysis. Figure 1*b* shows the channel in position for sample analysis. The electrical current to the coils was provided by a Xantrex HPD60-5 regulated DC power supply having a nominal maximum current of 5 A at 60 V (Xantrex Technology Inc., BC, Canada). It was controlled by computer using a general purpose interface bus interface (also from Xantrex Technology Inc.). The decay of the field during sample analysis could be programmed according to any desired function of time from a maximum of 0.71 T at the pole tips. The magnitude of the field at the position of the outer channel wall was monitored using a Model 6010 Gauss/Tesla meter (SYPRIS, Test & Measurement, F. W. Bell, Orlando, FL, USA). The field was recorded during the elution of samples at a position adjacent to the channel and a correction applied to obtain the field at the channel wall. The output of the Gauss meter was recorded to a data file using a 12 bit analogue-to-digital converter (DI-154RS, Dataq Instruments, Akron, OH, USA) and the company's WINDAQ LITE software.

The channel was machined to a depth of 250 μm into the surface of a precision-turned Delrin (du Pont) rod of 1.488 cm diameter and 15.49 cm length. The helical path made four complete revolutions around the rod. It had an overall length of 23.5 cm, and a breadth of about 1.6 cm, giving a nominal volume of 0.94 ml. The inlet and outlet ports were machined into the ends of the rod, and tapped for chromatography fittings. This work was carried out by Criterion Tool & Die, Inc. (Brook Park, OH, USA). The Delrin rod was inserted into a tightly fitting, internally polished stainless-steel (316 grade) tube of outer diameter 1.588 cm and wall thickness 0.051 cm. This was accomplished by cooling the two components in liquid nitrogen, assembling them and allowing the assembly to return to room temperature.

A Waters 515 high-performance liquid chromatography (HPLC) pump (Waters Corp., Milford, MA, USA) was used to provide the flow of fluid to the channel. The samples for analysis were introduced to the channel using a 7725i Rheodyne injection valve (Rheodyne, Cotati, CA, USA) with a 20 µl injection loop. A model VUV-12 HPLC UV detector (fixed wavelength 254 nm, HyperQuan, Inc., Colorado Springs, CO, USA) was used to detect the eluting particles at the channel outlet. The detector output was recorded to the data file using the same 12 bit analogue-to-digital converter as used for the Gauss meter.

The magnetic nanoparticle materials were kindly provided by Jurg Rohrer of BD Biosciences Pharmingen. They were obtained from Skold Technology, and are the type of particle used to manufacture the commercial IMag line of products used for cell separation. Two different lots (no. 78 and no. 80) of dextran-coated magnetite nanoparticles and one lot of uncoated magnetic nanoparticles suspended in 10 mM 2-(*N*-morpholino) ethanesulphonic acid (MES) buffer at pH 6.1, were examined. The dextran-coated particles had a nominal diameter range of 230 ± 150 nm, determined by dynamic light scattering. They were composed of single-domain magnetite nanoparticles distributed within the dextran coating. The uncoated particles were presumably the single-domain nanoparticles dispersed in the suspending medium, although there may have been some association. Before analysis, the coated samples were diluted 7 : 1 and the uncoated 14 : 1 in the phosphate buffered saline (PBS) used as carrier fluid. The PBS was degassed and filtered using a 0.22 µm pore Millipore filter prior to use. Every sample was sonicated for 1 min before analysis to help break up any aggregates that may have formed. To carry out an analysis, the field-decay program was set up on the computer, and the initial high field was applied to the channel. A 20 µl sample would then be introduced to the channel using the injection valve and a loading flow rate of 0.10 ml min^{-1} for 2 min to pass through the connecting tubing and onto the channel. The flow was then stopped for 15 or 30 min (depending on the initial field) to allow the particles to relax to their steady-state distributions. The carrier flow was then re-established at the desired flow rate for analysis, and the field-decay program initiated. Note that the pre-decay time t_1 of the conventional power program described by equation (2.7) was over-ridden and set to a time t_p for the reported experiments. For lot no. 80, the time t_p was fixed at 2 min, and for lot no. 78, t_p was fixed at 16 min. The field-decay program then followed the equation

$$B_\mathrm{o}(t) = B_\mathrm{o}(0)\left(\frac{t_1 - t_\mathrm{a}}{t - t_\mathrm{p} + t_1 - t_\mathrm{a}}\right)^p, \tag{3.1}$$

and the time constants t_1 and t_a are no longer independent parameters. The various flow rates and the field-decay parameters used for the set of analyses are listed in table 1. As explained earlier, the actual field was monitored during each sample analysis.

4. Results and discussion

Figure 2 shows an elution of the uncoated magnetic material. The field was programmed from an initial 46.1 mT at the accumulation wall, held constant for 2 min, and decreased to 4.8 mT over a period of 48 min. At this point, the channel

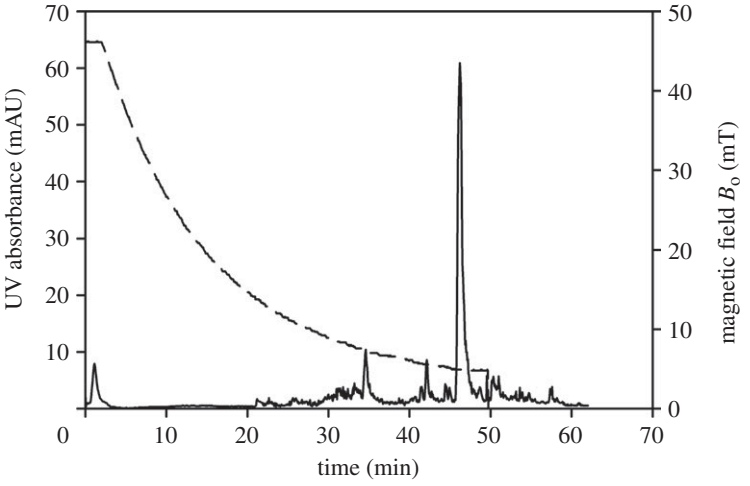

Figure 2. Elution of the uncoated magnetic nanoparticles under the programmed field decay. The magnetic field at the accumulation wall is plotted as the dashed curve and refers to the right-hand axis. Channel flow rate is $0.5\,\mathrm{ml\,min^{-1}}$.

Table 1. Parameters used for the reported experimental analyses.

	$B_o(0)$ (mT)	p	t_p (min)	$(t_1 - t_a)$ (min)	$\dot{V}$ ($\mathrm{ml\,min^{-1}}$)
lot no. 80					
(a)	55.0	4	2	20	1.0
(b)	53.1	4	2	20	0.5
(c)	53.8	12	2	104	0.5
(d)	56.7	8	2	108	0.5
lot no. 78					
(a)	54.1	6	16	56	0.5
(b)	232	6	16	56	0.5
(c)	560	6	16	56	0.5

was removed from the quadrupole aperture and the field dropped to effectively zero. The field at the accumulation wall is plotted as the dashed line in the figure and refers to the right-hand axis. A channel flow rate of $0.5\,\mathrm{ml\,min^{-1}}$ was used. The material does not elute as a broad peak, but as a series of spikes. This is an indication of strong aggregation of the material in the magnetic field. Data reduction would be meaningless for this sample.

Figure 3 shows the field-decay programs for the four analyses of lot no. 80. The field was recorded during each analysis at a point adjacent to the channel, and an adjustment made to estimate the magnitude of the field at the accumulation wall. It is these adjusted values of the measured field that are shown in the figure. The field-decay parameters for curves (a) and (b) were identical (table 1), and the small differences in measured field may be attributed

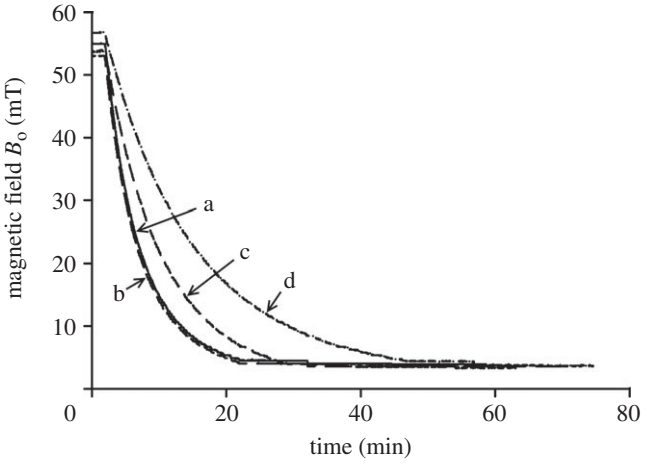

Figure 3. The field-decay programs monitored during analyses of lot no. 80. The field was measured adjacent to the channel, and an adjustment made to estimate the field at the channel accumulation wall. The curves correspond to the experimental parameters listed in table 1.

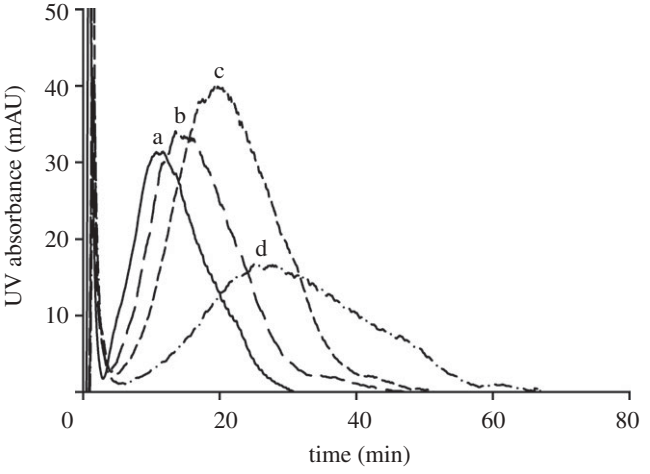

Figure 4. Fractograms for lot no. 80 obtained under the different experimental conditions listed in table 1.

to uncertainty in the precise positioning of the probe of the Gauss/Tesla meter. The channel flow rates for experiments (a) and (b) were different; a flow rate of $1.0\,\mathrm{ml\,min^{-1}}$ was used for (a), while $0.5\,\mathrm{ml\,min^{-1}}$ was used for (b), (c) and (d). In all four experiments, the field B_o decayed to a final level of between 3 and 4 mT. This corresponds to the remnant field of the quadrupole magnet pole tips, and so remained when the electrical current had dropped to zero. (Methods have since been developed to avoid this limitation, but these will be discussed elsewhere.) The four elution curves, or fractograms as they are known in the FFF literature, are shown in figure 4. For runs (a) and (b),

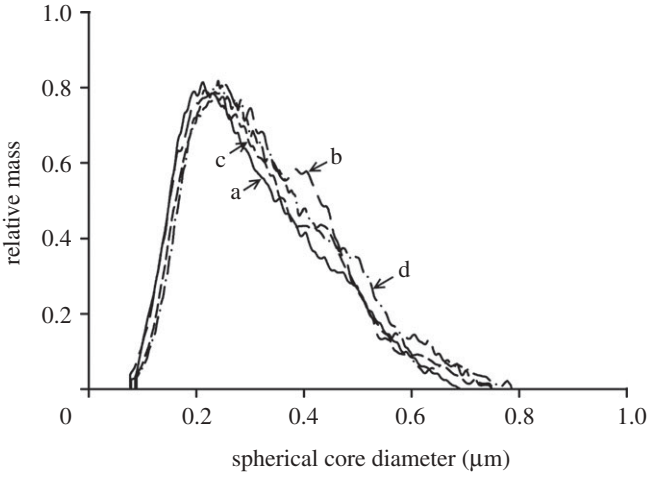

Figure 5. Distributions in equivalent spherical magnetite core diameter for lot no. 80 calculated from the fractograms shown in figure 4.

the field-decay program was almost identical, but the sample was eluted more quickly in run (a). This is due to the higher flow rate used for run (a) as compared with run (b). Run (c) shows a slower elution than run (b), and run (d) is slower than run (c). This is as expected and is due to the more slowly decaying field program used for these analyses. Each of the fractograms shows a sharp initial peak known as the void peak corresponding to the elution of non-retained material in the sample. This is followed by a broad peak corresponding to the elution of the particle sample. The material eluted in the void peak is too weakly retained to yield meaningful data, and the data reduction effectively starts from the bottom of the valley between the two peaks. The precise approach to selection of the initial data point is described by Williams *et al.* (2001).

Figure 5 shows the calculated mass distributions as functions of the equivalent spherical magnetite core diameters for the four analyses. Note that no light-scattering corrections were made, as explained earlier, so that the detector response is effectively assumed to be proportional to particle mass concentration. Also, a magnetization curve was assumed in order to carry out the data reduction. This is given by the equation

$$M = \frac{9.152 \times 10^6 B}{1 + 27.30B - 0.9229B^2}, \tag{4.1}$$

where M has units of $\mathrm{A\,m^{-1}}$ and B units of T. The curve was taken from the literature (Yamaura *et al.* 2004), and is representative for magnetite nanoparticles. (The conversion of units to SI was made as follows: $1\,\mathrm{emu\,g^{-1}} = \rho_\mathrm{m}\,\mathrm{emu\,ml^{-1}} = \rho_\mathrm{m} \times 10^3\,\mathrm{A\,m^{-1}}$, where ρ_m is the density of magnetite, taken to be $5.24\,\mathrm{g\,ml^{-1}}$ and $10^4\,\mathrm{Oe} = 1\,\mathrm{T}$.) Again, the same magnetization curve was assumed for all transformations, so that the results may be compared directly with one another. The mass distributions are very similar. There is no trend in calculated

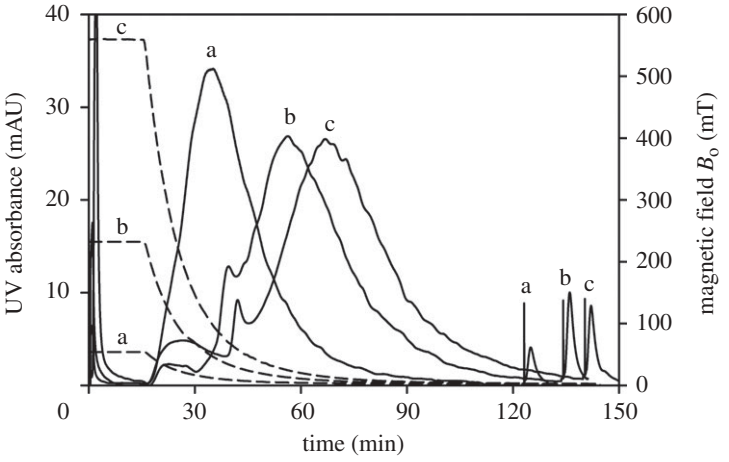

Figure 6. Fractograms for lot no. 78 obtained under the conditions listed in table 1. The dashed curves refer to the right-hand axis and show the decay of the field at the channel accumulation wall.

size distributions for runs (b), (c) and (d), for example, for which the flow rate is identical, but the field decay becomes successively slower. The differences may be explained by uncertainty in the placing of the Gauss/Tesla meter probe, and consequent uncertainty in the field measurement.

Figure 6 shows three fractograms for lot no. 78, obtained at the same flow rate of $0.5\,\mathrm{ml\,min^{-1}}$, identical time constants and power for the field decay, but different initial fields. The conditions are listed in table 1. The identical program time constants and power means that the relative change in field with time is identical for each run. It is not surprising that run (a), corresponding to the lowest field conditions, shows the fastest elution, followed by (b) and (c). For these experiments, the field at the accumulation wall approached a level of between 2 and 3 mT, even from the highest initial field of 560 mT. However, in each case, the channel was removed from the magnet aperture at a time indicated by the spike on each fractogram. The field may be assumed to drop effectively to zero at this point, and in every case, a small amount of material was subsequently eluted from the channel. This must represent strongly retained and perhaps aggregated material. The majority of the material eluted during the programmed field decays, however, and the fractograms were transformed to the mass distributions shown in figure 7. Again, the distributions do not differ from one another significantly, except in the region of the lower core sizes. This is to be expected because, at the lowest initial field, the field gradient is not sufficient to retain the particles having the smallest magnetite content. These would be eluted with the void peak, and would not be included in the data-reduction procedure. At the highest initial field, particles containing less magnetite are retained in the channel, and elute under the conditions of the programmed field decay. They are therefore represented in the distribution curves. The differences at the higher extreme of magnetite content are a little more complicated to explain. The data reduction included a simple steric correction consistent with equation (2.6) where α was assumed to be the ratio of $d_\mathrm{m}/2w$. This is a first-order correction for finite particle size, and does not even account for the dextran component. At high elution times, the

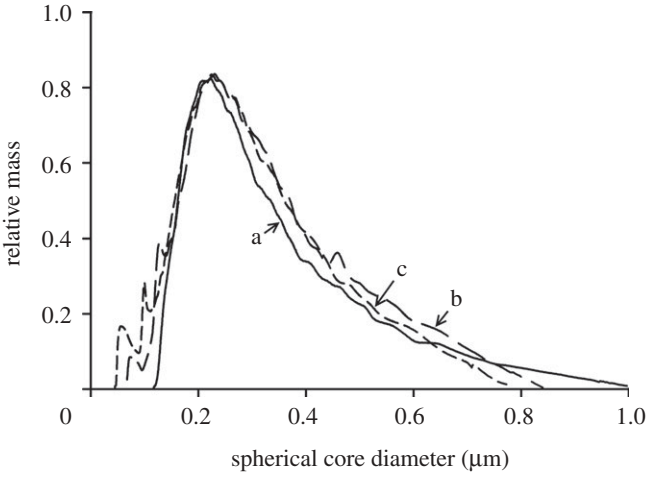

Figure 7. Distributions in equivalent spherical magnetite core diameter for lot no. 78 calculated from the fractograms shown in figure 6.

contribution to retention ratio owing to the steric correction is most significant, and the association of core diameters to these high elution times will therefore be most uncertain. The differences in the distributions at the upper extremes of core diameters are almost certainly an artefact of the first-order steric correction.

5. Conclusions

The aggregation of the uncoated magnetite nanoparticles in the magnetic field is evident from the intermittent elution of material shown in figure 2. Equation (2.15) may be used to calculate a coupling constant λ_{cc} for 10 nm magnetite particles (estimated size of the single-domain particles). If we assume a saturation magnetization of magnetite of $360\,\mathrm{kA\,m^{-1}}$, and thermal energy kT of 4.1×10^{-21} J, the value of λ_{cc} is calculated to be 1.7. The particles are single domain and will have permanent magnetization of around $360\,\mathrm{kA\,m^{-1}}$. They could be expected to interact with one another without applying a magnetic field. They are kept in stable suspension only with the aid of surfactant. It is not surprising that dipole–dipole interaction of these particles occurs in the magnetic field.

The experiments involving the dextran-coated samples did not indicate any strong influence of experimental parameters on the calculated distributions in magnetite content. In fact, the results were remarkably consistent. The absolute ranges for the calculated core diameters do seem to be somewhat larger than expected, however, given the nominal hydrodynamic diameter range of 80–380 nm. The calculations were based on an assumed magnetization curve, but the actual magnetization could not have been significantly higher than this assumed curve. The results could be interpreted as evidence for magnetic dipole interaction of the particles in the magnetic field, particularly for those particles incorporating the highest amounts of magnetite. These may interact at the high initial field and become immobilized on the channel wall. As the field decreased, the particle

magnetic moments would decrease and their interaction become weaker. At some point, they may be released from their interaction at the wall and start their migration along the channel. In this way, their elution times would be longer than predicted by ideal FFF theory (which does not account for particle–particle interactions). The longer elution times would result in the calculated magnetite content being higher than expected. If this is the case, however, the interactions and capture and release of the larger particles would have to occur in a very reproducible manner. It is apparent that further experiments are required in order to determine the extent and nature of perturbations to elution in QMgFFF.

This work was supported by grants CTS-0125657 from the National Science Foundation and R01 CA62349 from the National Institutes of Health. The authors also thank Jurg Rohrer of BD Biosciences Pharmingen for kindly supplying the magnetic nanoparticle samples used in this work.

References

Calderón, O. G. & Melle, S. 2002 Dynamics of simple magnetorheological suspensions under rotating magnetic fields with modulated Mason number. *J. Phys. D: Appl. Phys.* **35**, 2492–2498. (doi:10.1088/0022-3727/35/20/305)

Carpino, F., Moore, L. R., Chalmers, J. J., Zborowski, M. & Williams, P. S. 2005*a* Quadrupole magnetic field-flow fractionation for the analysis of magnetic nanoparticles. *J. Phys. Conf. Ser.* **17**, 174–180. (doi:10.1088/1742-6596/17/1/024)

Carpino, F., Moore, L. R., Zborowski, M., Chalmers, J. J. & Williams, P. S. 2005*b* Analysis of magnetic nanoparticles using quadrupole magnetic field-flow fractionation. *J. Magn. Magn. Mater.* **293**, 546–552 (doi:10.1016/j.jmmm.2005.01.071)

Carpino, F., Zborowski, M. & Williams, P. S. 2007 Quadrupole magnetic field-flow fractionation: a novel technique for the characterization of magnetic nanoparticles. *J. Magn. Magn. Mater.* **311**, 383–387. (doi:10.1016/j.jmmm.2006.11.162)

Chantrell, R. W., Bradbury, A., Popplewell, J. & Charles, S. W. 1982 Agglomerate formation in a magnetic fluid. *J. Appl. Phys.* **53**, 2742–2744. (doi:10.1063/1.330953)

de Gennes, P. G. & Pincus, P. A. 1970 Pair correlations in a ferromagnetic colloid. *Phys. Kondensierten Materie* **11**, 189–198. (doi:10.1007/BF02422637)

Gast, A. P. & Zukoski, C. F. 1989 Electrorheological fluids as colloidal suspensions. *Adv. Colloid Interface Sci.* **30**, 153–202. (doi:10.1016/0001-8686(89)80006-5)

Giddings, J. C. 1966 A new separation concept based on a coupling of concentration and flow nonuniformities. *Sep. Sci. Technol.* **1**, 123–125. (doi:10.1080/01496396608049439)

Giddings, J. C. 1978 Displacement and dispersion of particles of finite size in flow channels with lateral forces. Field-flow fractionation and hydrodynamic chromatography. *Sep. Sci. Technol.* **13**, 241–254. (doi:10.1080/01496397808060222)

Giddings, J. C. 1979 ERRATA. Displacement and dispersion of particles of finite size in flow channels with lateral forces. Field-flow fractionation and hydrodynamic chromatography. *Sep. Sci. Technol.* **14**, 869–870. (doi:10.1080/01496397908060246)

Giddings, J. C. 1984 Field-flow fractionation. *Sep. Sci. Technol.* **19**, 831–847. (doi:10.1080/01496398408068596)

Giddings, J. C. 1993 Field-flow fractionation: analysis of macromolecular, colloidal, and particulate materials. *Science* **260**, 1456–1465. (doi:10.1126/science.8502990)

Giddings, J. C. 2000 The field-flow fractionation family: underlying principles. In *Field-flow fractionation handbook* (eds M. E. Schimpf, K. Caldwell & J. C. Giddings), pp. 3–30. New York, NY: John Wiley & Sons.

Giddings, J. C., Williams, P. S. & Beckett, R. 1987 Fractionating power in programmed field-flow fractionation: exponential sedimentation field decay. *Anal. Chem.* **59**, 28–37. (doi:10.1021/ac00128a007)

Goldman, A. J., Cox, R. G. & Brenner, H. 1967 Slow viscous motion of a sphere parallel to a plane wall—II Couette flow. *Chem. Eng. Sci.* **22**, 653–660. (doi:10.1016/0009-2509(67)80048-4)

Hansen, M. E. & Giddings, J. C. 1989 Retention perturbations due to particle-wall interactions in sedimentation field-flow fractionation. *Anal. Chem.* **61**, 811–819. (doi:10.1021/ac00183a006)

Hansen, M. E., Giddings, J. C. & Beckett, R. 1989 Colloid characterization by sedimentation field-flow fractionation. VI. Perturbations due to overloading and electrostatic repulsion. *J. Colloid Interface Sci.* **132**, 300–312. (doi:10.1016/0021-9797(89)90245-2)

Hayes, C. F. 1975 Observation of association in a ferromagnetic colloid. *J. Colloid Interface Sci.* **52**, 239–243. (doi:10.1016/0021-9797(75)90194-0)

Jeffery, G. B. 1922 The motion of ellipsoidal particles immersed in a viscous fluid. *Proc. R. Soc. Lond. A* **102**, 161–179. (doi:10.1098/rspa.1922.0078)

Jönsson, J. Å. & Carlshaf, A. 1989 Flow field flow fractionation in hollow cylindrical fibers. *Anal. Chem.* **61**, 11–18. (doi:10.1021/ac00176a004)

Jordan, P. C. 1973 Association phenomena in a ferromagnetic colloid. *Mol. Phys.* **25**, 961–973. (doi:10.1080/00268977300100821)

Kirkland, J. J., Rementer, S. W. & Yau, W. W. 1981 Time-delayed exponential field-programmed sedimentation field flow fractionation for particle-size-distribution analyses. *Anal. Chem.* **53**, 1730–1736. (doi:10.1021/ac00235a005)

Latham, A. H., Freitas, R. S., Schiffer, P. & Williams, M. E. 2005 Capillary magnetic field flow fractionation and analysis of magnetic nanoparticles. *Anal. Chem.* **77**, 5055–5062. (doi:10.1021/ac050611f)

Martin, J. E. & Anderson, R. A. 1996 Chain model of electrorheology. *J. Chem. Phys.* **104**, 4814–4827. (doi:10.1063/1.471176)

Martin, M., Myers, M. N. & Giddings, J. C. 1979 Nonequilibrium and polydispersity peak broadening in thermal field-flow fractionation. *J. Liq. Chromatogr.* **2**, 147–164. (doi:10.1080/01483917908060055)

Melle, S., Fuller, G. G. & Rubio, M. A. 2000 Structure and dynamics of magnetorheological fluids in rotating magnetic fields. *Phys. Rev. E* **61**, 4111–4117. (doi:10.1103/PhysRevE.61.4111)

Melle, S., Rubio, M. A. & Fuller, G. G. 2001 Erratum: structure and dynamics of magnetorheological fluids in rotating magnetic fields. *Phys. Rev. E* **63**, 059902. [Erratum in *Phys. Rev. E* 2000 **61**, 4111]. (doi:10.1103/PhysRevE.63.059902)

Melle, S., Calderón, O. G., Fuller, G. G. & Rubio, M. A. 2002*a* Polarizable particle aggregation under rotating magnetic fields using scattering dichroism. *J. Colloid Interface Sci.* **247**, 200–209. (doi:10.1006/jcis.2001.8087)

Melle, S., Calderón, O. G., Rubio, M. A. & Fuller, G. G. 2002*b* Rotational dynamics in dipolar colloidal suspensions: video microscopy experiments and simulations results. *J. Non-Newtonian Fluid Mech.* **102**, 135–148. (doi:10.1016/S0377-0257(01)00174-4)

Melle, S., Calderón, O. G., Rubio, M. A. & Fuller, G. G. 2003 Microstructure evolution in magnetorheological suspensions governed by Mason number. *Phys. Rev. E* **68**, 041503. (doi:10.1103/PhysRevE.68.041503)

Mori, S. 1986 Magnetic field-flow fractionation using capillary tubing. *Chromatographia* **21**, 642–644. (doi:10.1007/BF02311919)

Reschiglian, P., Zattoni, A., Roda, B., Cinque, L., Parisi, D., Roda, A., Piaz, F. D., Moon, M. H. & Min, B. R. 2005 On-line hollow-fiber flow field-flow fractionation-electrospray ionization/time-of-flight mass spectrometry of intact proteins. *Anal. Chem.* **77**, 47–56. (doi:10.1021/ac048898o)

Rosensweig, R. E. 1997 *Ferrohydrodynamics*. Mineola, NY: Dover Publications, Inc.

Schimpf, M. E., Williams, P. S. & Giddings, J. C. 1989 Accurate molecular weight distribution of polymers using thermal field-flow fractionation with deconvolution to remove system dispersion. *J. Appl. Polym. Sci.* **37**, 2059–2076. (doi:10.1002/app.1989.070370725)

Vickrey, T. M. & Garcia-Ramirez, J. A. 1980 Magnetic field-flow fractionation: theoretical basis. *Sep. Sci. Technol.* **15**, 1297–1304. (doi:10.1080/01496398008068506)

Volkova, O., Cutillas, S. & Bossis, G. 1999 Shear banded flows and nematic-to-isotropic transition in ER and MR fluids. *Phys. Rev. Lett.* **82**, 233–236. (doi:10.1103/PhysRevLett.82.233)

Wijnhoven, J. E. G. J., Koorn, J. P., Poppe, H. & Kok, W. T. 1995 Hollow-fibre flow field-flow fractionation of polystyrene sulphonates. *J. Chromatogr. A* **699**, 119–129. (doi:10.1016/0021-9673(95)00172-J)

Williams, P. S. & Giddings, J. C. 1987 Power programmed field-flow fractionation: a new program form for improved uniformity of fractionating power. *Anal. Chem.* **59**, 2038–2044. (doi:10.1021/ac00144a007)

Williams, P. S. & Giddings, J. C. 1991 Comparison of power and exponential field programming in field-flow fractionation. *J. Chromatogr.* **550**, 787–797. (doi:10.1016/S0021-9673(01)88582-4)

Williams, P. S. & Giddings, J. C. 1994 Theory of field-programmed field-flow fractionation with corrections for steric effects. *Anal. Chem.* **66**, 4215–4228. (doi:10.1021/ac00095a017)

Williams, P. S., Giddings, J. C. & Beckett, R. 1987 Fractionating power in sedimentation field-flow fractionation with linear and parabolic field decay programming. *J. Liq. Chromatogr.* **10**, 1961–1998. (doi:10.1080/01483918708066808)

Williams, P. S., Xu, Y., Reschiglian, P. & Giddings, J. C. 1997 Colloid characterization by sedimentation field-flow fractionation: correction for particle-wall interaction. *Anal. Chem.* **69**, 349–360. (doi:10.1021/ac9606012)

Williams, P. S., Giddings, M. C. & Giddings, J. C. 2001 A data analysis algorithm for programmed field-flow fractionation. *Anal. Chem.* **73**, 4202–4211. (doi:10.1021/ac010305b)

Williams, P. S., Moore, L. R., Chalmers, J. J. & Zborowski, M. 2002 The potential of quadrupole magnetic field-flow fractionation for determining particle magnetization distributions. *Eur. Cells Mater.* **3**(Suppl. 2), 203–205.

Williams, P. S., Carpino, F. & Zborowski, M. 2009*a* Magnetic nanoparticle drug carriers and their study by quadrupole magnetic field-flow fractionation. *Mol. Pharm.* **6**, 1290–1306. (doi:10.1021/mp900018v)

Williams, P. S., Carpino, F. & Zborowski, M. 2009*b* Theory for nanoparticle retention time in the helical channel of quadrupole magnetic field-flow fractionation. *J. Magn. Magn. Mater.* **321**, 1446–1451. (doi:10.1016/j.jmmm.2009.02.065)

Yamaura, M., Camilo, R. L., Sampaio, L. C., Macêdo, M. A., Nakamura, M. & Toma, H. E. 2004 Preparation and characterization of (3-aminopropyl) triethoxysilane-coated magnetite nanoparticles. *J. Magn. Magn. Mater.* **279**, 210–217. (doi:10.1016/j.jmmm.2004.01.094)

Yang, F. J. F., Myers, M. N. & Giddings, J. C. 1974 Programmed sedimentation field-flow fractionation. *Anal. Chem.* **46**, 1924–1930. (doi:10.1021/ac60349a009)

Yau, W. W. & Kirkland, J. J. 1981 Retention characteristics of time-delayed exponential field-programmed sedimentation field-flow fractionation. *Sep. Sci. Technol.* **16**, 577–605. (doi:10.1080/01496398108058118)

Zborowski, M. 1997 Physics of the magnetic cell sorting. In *Scientific and clinical applications of magnetic carriers* (eds U. Häfeli, W. Schütt, J. Teller & M. Zborowski), pp. 205–231. New York, NY: Plenum Press.

Zborowski, M., Sun, L., Moore, L. R., Williams, P. S. & Chalmers, J. J. 1999 Continuous cell separation using novel magnetic quadrupole flow sorter. *J. Magn. Magn. Mater.* **194**, 224–230. (doi:10.1016/S0304-8853(98)00581-2)